Thermal expansion behavior of new Co-based alloys and implications for coatings

R. Wesley Jackson, Michael S. Titus, Matthew R. Begley, Tresa M. Pollock

PII: S0257-8972(15)30513-2
DOI: doi: 10.1016/j.surfcoat.2015.12.083
Reference: SCT 20839

To appear in: *Surface & Coatings Technology*

Received date: 23 September 2015
Revised date: 26 December 2015
Accepted date: 28 December 2015

Please cite this article as: R. Wesley Jackson, Michael S. Titus, Matthew R. Begley, Tresa M. Pollock, Thermal expansion behavior of new Co-based alloys and implications for coatings, *Surface & Coatings Technology* (2016), doi: 10.1016/j.surfcoat.2015.12.083

Thermal expansion behavior of new Co-based alloys and implications for coatings

R. Wesley Jackson[a,*], Michael S. Titus[a,**], Matthew R. Begley[a,b], Tresa M. Pollock[a]

[a] *Materials Department, University of California Santa Barbara, Santa Barbara, CA 93106-5050, USA*
[b] *Department of Mechanical Engineering, University of California Santa Barbara, Santa Barbara, CA 93106-5050, USA*

Abstract

The thermal expansion behavior of five γ'-($L1_2$) containing Co-based superalloys was measured using push-rod dilatometry. These results were analyzed to determine the mean coefficient of thermal expansion (CTE), the instantaneous CTE, and γ'-solvus temperature of the alloys. The CTE was found to depend strongly on the γ'-solvus temperature.

In turbine applications, these alloys will be part of a multilayer system that generates thermal stresses due to the CTE mismatch between the components. To investigate this phenomenon, the CTE data was incorporated into a thermo-mechanical model to calculate the energy release rate (ERR) for the delamination of coatings from these alloys. The ERR of a thermally grown oxide (TGO) formed on the bare and bond coated Co-based alloys was determined as a function of superalloy and bond coat CTE. The ERR of a thermal barrier coating (TBC) was evaluated as a function of temperature, superalloy CTE, and coating thickness. The ERR was found to be about 1.5× greater in Co-based superalloys compared to Ni-based superalloys cooled from $T = 1100\,^{\circ}\mathrm{C}$ to ambient. Strategies for reducing the driving force for delamination are discussed.

Keywords: cobalt; superalloy, thermal expansion (CTE); thermal barrier coating (TBC); delamination;

*Corresponding Author: Tel +1 412 523 3373; Fax +1 805 893 8486;
e-mail: rwesleyjackson@engineering.ucsb.edu
**Corresponding Author: Tel +1 805 893 2883; Fax +1 805 893 8486;
e-mail: mtitus@engineering.ucsb.edu

1. Introduction

The drive to increase the operating temperature of gas turbine engines has motivated the development of superalloys capable of withstanding higher temperatures [1]. The discovery of a γ'-$L1_2$ phase in the Co-Al-W system has enabled a new class of precipitation-strengthened superalloys, which could increase the operating temperature of gas turbine engines [2–4]. Indeed, new $L1_2$-containing Co-based superalloys of relatively simple chemistries have recently been observed to exhibit comparable and, in some cases, superior high-temperature creep properties compared to 1st-generation Ni-based superalloys [5–8]. While these Co-based superalloys have higher density compared to Ni-based alloys, their higher specific modulus (E/ρ) makes these new materials suitable candidates for both aero-engine and industrial gas turbines [9]. Further, the ability of Co-based superalloys to resist casting defects during single crystal solidification makes them attractive candidates for large-scale components used in industrial engines [10].

The durability of superalloy components is strongly affected by their oxidation rate. As such, the chemistries of commercial Ni-based superalloys have been tailored to minimize alloy consumption by oxidation through formation of a slowly growing and adherent oxide scale [1, 11]. Ideally, α-Al_2O_3 exclusively forms, but transient oxides (e.g. NiO, CoO, $(Ni,Co)(Al,Cr)_2O_4$) can form prior to protective alumina formation in many alloys [11, 12]. Rapid metal loss can result from the spallation and regrowth of the TGO. The driving force for spallation increases with the thermally grown oxide (TGO) thickness and is accelerated when the growth rate of the TGO increases when oxides other than alumina grow [13].

When higher temperature exposures are required, these components are then coated with an aluminum rich bond coat and a ceramic thermal barrier coating (TBC), typically 7 wt.% Y_2O_3 stabilized ZrO_2, 7YSZ. In land-based turbines, both of these coatings are typically applied through plasma spray processes. The bond coat is commonly applied via a low-pressure plasma spray (LPPS) process, and adequate mechanical adhesion of the TBC is obtained by a relatively high root-mean-squared roughness of the bond coat, which is on the order of 10 µm [14]. The TBC is typically deposited through an air plasma spray (APS) process that is tailored to impart high in-plane compliance, which results from either high porosity or an array of through-thickness cracks. The coating typically fails as a result of

cracks growing in the TBC directly above the TGO [15, 16]. Since the failure processes are driven by the CTE mismatch with the superalloy substrate, it is essential to understand the CTE behavior of new alloy classes.

This paper reports the coefficient of the thermal expansion (CTE) for five $L1_2$-containing Co-based superalloys. This data is then incorporated into a thermo-mechanical model to evaluate the driving force for TGO delamination from these superalloys and for cracking in TBC systems. The implications of composition-dependent CTE and their relation to the γ'-solvus are discussed.

2. Material and Experimental Procedures

Five alloy compositions,Table 1, were vacuum induction melted by Sophisticated Alloys, Inc. All alloy compositions lie within, or very near to, the γ-γ' (A1-$L1_2$) phase field at 900 °C [17]. Prior to dilatometry measurements, all Co-based alloys were subjected to a solution heat treatment of 1225 °C for 60 h so that a compositionally-homogenized γ phase was achieved. The CoNi-based alloys were subjected to solution heat treatments of 1215 °C for 12 h. Additionally, the properties of the single crystal Ni-base superalloy René N5 were investigated for comparative purposes. Backscatter SEM micrographs of the Ternary and CoNi-A alloys in Figure 1 show the cubical γ' precipitates in a γ matrix, typical of superalloys.

Specimens approximately 10 mm in diameter and 25 mm in length were machined via electrical discharge machining (EDM) and used for push-rod dilatometry experiments. Subsequent mechanical grinding removed any surface damage due to the EDM process. A final grit of 800 was used to achieve sufficient surface finish. All specimens were ultrasonically cleaned in an acetone bath prior to dilatometry experiments. Each alloy was tested 2-3 times to ensure consistency in the measurement. Data from the second heating cycle was typically used for subsequent analysis.

Thermal expansion measurements were conducted using an Orton 2016HU dilatometer equipped with a sealed quartz tube, R-type thermocouple, and a linear voltage displacement transducer used to measure specimen elongation. In order to prevent significant oxidation, a reducing gas of Ar-5%H_2 was flowed through the quartz tube containing the specimens during the experiment.

An α-Al_2O_3 standard from Orton of similar dimensions was used in order to ensure proper calibration of the CTE measurements. All CTE experiments were conducted using a 3 K/min heating and cooling ramp up to a temperature of at least 20 °C greater than the γ'-solvus of the alloys. Measurements of specimen displacement were taken every 1°C.

3. Determination of the mean CTE, α, instantaneous CTE $\hat{\alpha}$, and γ'-solvus

All CTE data presented were derived from calibrated heating data of the thermal strain, $\Delta L/L_0$ vs. T, where ΔL is the difference between the specimen length L at temperature T and the initial specimen length at 25° C, L_0. The thermal strain of the Ternary and 6Ti alloys are presented in Figure 2. The mean thermal expansion coefficients[1], α (often referred to as the engineering CTE or secant CTE) from 25 °C was determined by:

$$\alpha(T) = \frac{\Delta L/L_0}{T - 25\,^{\circ}C} \tag{1}$$

The mean CTE data was fit to a 4^{th} order polynomial and the expressions are listed in Table 2.

The instantaneous CTE, $\hat{\alpha}$, was calculated by:

$$\hat{\alpha}(T) = \frac{d\,(\Delta L/L)}{dT} \tag{2}$$

where the derivative of the curve was determined by calculating the average slope over the range ±10°C of a given temperature. The mean CTE and instantaneous CTE of the five Co-based superalloys and the Ni-based superalloy René N5 are plotted in Figure 3.

Both the mean and instantaneous CTE increase smoothly with temperature until the γ'-solvus, at which an inflection point in the curves occurs. The γ'-solvus was determined by fitting the mean CTE data above and below the inflection point to a linear expression

[1]When measurements were initiated above room temperature, the sample length at 25°C was calculated by extrapolating the $\Delta L/L_0$ vs. T to 25 °C. The expansion of the sample from the initial test temperature to room temperature, ϵ_{RT} is then inserted into Equation 2 so that thermal strains are referenced to 25°C.

$$\alpha(T) = \frac{\Delta L/L_0 + \epsilon_{RT}}{T - 25\,^{\circ}C}$$

and then finding the intersection of the these two lines, as shown in the inset of Figure 3(a) [18]. The γ'-solvi determined from these curves for the Ternary, 2Ta, 6Ti, and CoNi-A alloys are listed in Table 2. These results are in general agreement with the transformation temperatures determined through differential thermal analysis in Refs. [6, 7, 19]. The γ'-solvus of the CoNI-E alloy and René N5 were taken from the literature because the transformation temperatures were too high for experimental determination. Additionally, the solidus temperature of each alloy, T_m, was taken from the literature and is listed in Table 2 [19, 20].

4. Effect of temperature and composition on the CTE of γ-γ'superalloys

There has been limited investigation of the CTE of $L1_2$-containing Co-based superalloys [5, 21], but work on systems with similar characteristics can be used as a starting point in understanding the effect temperature and composition have on CTE. Generally, the CTE of single phase alloys increases continuously with temperature [22], and the CTE of two phase alloys depends primarily on the CTE and volume fraction of the two constituent phases. In the Ni-based superalloys, the CTE of the Ni_3Al-($L1_2$) phase is lower than the FCC solid solution phase, and the volume fraction of the $L1_2$ phase decreases with temperature, reaching complete dissolution at the γ'-solvus. As a result, the CTE of a precipitate-containing alloy such as René N5 is expected to increase with increasing temperature, Figure 3.

The temperature dependence of the Co-based alloys is qualitatively similar to the Ni-based alloy René N5. The instantaneous CTE curves in Figure 3(b) and (d) show that $\hat{\alpha}$ moderately increases until approximately 200°C below the γ'-solvus when the instantaneous CTE increases rapidly. Thus, the CTEs of both types of alloys tend to scale with γ'-solvus temperature. However, changes in alloy composition can alter the $L1_2$ volume fraction in the alloy as well as the CTE of the γ and γ' phases. The CTE of the 6Ti is 1 ppmK^{-1} higher than the Ternary and 2Ta alloys at low temperatures, so despite having a higher γ'-solvus, α_{6Ti} is higher than the $\alpha_{Ternary}$ and α_{2Ta} until 950°C and 1050°C, respectively. Interestingly, the CTE of the CoNi-A alloy begins increasing markedly well below γ'-solvus, and the CoNi-E alloy exhibits a lower mean CTE compared to René N5.

5. Delamination of coatings on $L1_2$ containing superalloys

The durability of superalloy components in turbine engines depends critically on the ability of ceramic coatings and/or the thermally grown oxide to remain adherent during operation. Arguably, the principle mechanism of coating failure is delamination, in which the stored elastic energy in the coating drives separation from the substrate. Delamination occurs when the strain energy released by the advance of an interface crack (defined as the energy release rate (ERR), G) reaches a critical value (defined as the interface toughness, Γ) [23].

In the subsequent analysis, we quantify the ERR associated with the advance of a semi-infinite interface flaw, which represents an upper bound to the driving force for debonding. The steady-state energy release rate for interface delamination can be computed from the difference in stored elastic strain energy in the multilayers ahead of the interface crack and those behind the crack. The results reported were generated using the conventional approach for multilayers [23], which invokes the following assumptions: (1) the materials are isotropic and purely elastic, with the stress-free state defining the reference temperature for thermal strains, taken to be the elevated operating temperature, (2) any multilayer (i.e. either the original complete stack or new multilayers created by the interface crack) experiences a linear strain distribution as consistent with Bernoulli-Euler bending, and (3) there are no externally applied loads or constraints that resist elongation or bending of any given multilayer. This approach is a rigorous generalization of the bilayer results described in [23]; complete details of the generalization are given in [24] for multilayers with an arbitrary number of layers.[2]

The results presented here represent the complete solutions for G that account for the influence of all layers, including all mean CTEs, α, moduli, E, and layer thicknesses, H. However, as is well established for coatings on substrates that are comparatively thick and sufficiently stiff, the thermal misfit strains between the layers that experience delamination and the substrate dominate the response. The misfit strain in a given layer is defined as $(\alpha_s(T) - \alpha_c(T))\,(T - T_o)$, where α_s is the substrate mean CTE, α_c is the mean CTE of the

[2]Codes to repeat the calculations are freely available. <http://www.engineering.ucsb.edu/~begley/LayerSlayer.html>

layer in question, T is the current temperature and T_o is the temperature at which the misfit strains are zero. Because the misfit strain in the delaminating layer dictates the strain energy stored that is released by crack advance in the film ahead of the delamination, the misfit strain with the substrate dominates G. The misfit strains in layers that do not delaminate play a secondary role.

To extend this analysis to predict failure, the toughness of the delaminating interfaces would need to be determined, which, can depend sensitively on the chemistry of the interface [25]. However, the concentration of impurities (*e.g.* S, C) and reactive elements (*e.g.* Y, Hf, Zr) typically have a stronger effect on interfacial toughness than the bulk alloy constituents [26]. As a result, processing and alloy purity are expected to play a dominant role in determining the interfacial toughness, rather the bulk composition and are beyond the scope of this paper.

Additionally, the deformation field (stress state/ elastic properties) around the crack tip can strongly influence the toughness [23]. Generally, the crack-tip displacements are decomposed into opening (mode I) and sliding (mode II) components with the toughness increasing with the proportion of sliding displacements. However, as the coatings are under large compressive stresses, the crack-tips are exclusively mode II in character [24, 27].

5.1. Delamination of oxidized superalloys

Oxide scales grow on the surface of superalloys during high temperature exposure. Large compressive stresses tend to develop in the TGO during cooling due to the inherent CTE mismatch between the TGO and the superalloy. The driving force for delamination, the stored elastic strain energy, is proportional to the TGO thickness and as a result the durability of the oxide scale improves as the growth rate decreases. Thus, ideally, the TGO is exclusively slowly growing Al_2O_3. However, transient oxides such as CoO or spinel can form prior to exclusive alumina formation [4, 28].

The thermo-mechanical model was used to determine the energy release rate, G, for these oxides on superalloy substrate. Calculations of the ERR at 25°C following cooling from 1100°C were made for a single layer TGO composed of Al_2O_3 and a bilayer TGO with a CoO layer above the Al_2O_3. G is plotted as a function of substrate mean CTE in Figure 4(a) for

both scenarios. As the CTE of the superalloy increases, so does the CTE mismatch, which increases the magnitude of the compressive stresses in the TGO. For example, increasing α_{alloy} from 16 ppmK^{-1} to 19 ppmK^{-1} (e.g CoNi-E to Ternary) increases the stress in the TGO from -4.7 GPa to -6.7 GPa and doubles G at 1100°C. Further, calculations of the deformation field indicates that the delamination propagates in a strictly mode II character for each of the alloys [24, 27].

Calculations were also performed for a bilayer Al_2O_3-CoO TGO, where $H_{Al_2O_3}$=3 µm and H_{CoO}=10 µm, because such a scale may form when transient CoO growth occurs prior to the formation of a continuous Al_2O_3 scale [4, 11, 12]. This oxide morphology is common in alloys with low Al concentration [29, 30]. Because the mean CTE of CoO (15 ppmK^{-1}) is much higher than Al_2O_3 (8 ppmK^{-}1), G for cracking the thicker bilayer scale is actually less than G for the Al_2O_3 only TGO for superalloy CTEs less than 18 ppmK^{-1}. G of the bilayer TGO surpasses G of the Al_2O_3 TGO when α_{alloy} exceeds 18 ppmK^{-1}, and the differences in G grow monotonically with increasing α_{alloy}, as shown in Figure 4a. The values of G for delamination of the single and bilayer TGO from each of the 6 alloys are presented in the bar chart in Figure 4(b).

5.2. TGO delamination from bond coated superalloys

In applications in which a component will experience higher temperatures, the intrinsic oxidation resistance of the superalloy may be insufficient, necessitating the application of an aluminum rich bond coat. The durability of these bond coatings is strongly affected by composition and processing method [15, 31, 32]. In industrial gas turbines, γ-β NiCoCrAlY bond coats are commonly used due to their processability and high ductility at low temperatures. Taylor and Walsh [33] and Haynes and co-workers [34] have determined mean CTE of a number of these alloys finding that the CTE ranges from 15-20 ppmK^{-1} at 1100°C, depending on alloy composition.

The effect of bond coat CTE on the driving force for the delamination of the TGO was analyzed for bond coated CoNi-A and CoNi-E superalloys. The driving force for delamination of a 3 µm-thick Al_2O_3 TGO grown on a 100 µm-thick bond coat on a 3 mm-thick superalloy was determined and is plotted in Figure 5. In contrast to the variation of the superalloy

CTE, little change in G was observed as a function of bond coat CTE, Figure 5. For example, increasing the mean CTE of the superalloy from 15 to 20 ppmK^{-1} increases G by nearly a factor of 3, while the same change in CTE of the bond coat only raises G by 10%. This is due to the fact that the bond coat is less than 3% of the thickness of the superalloy, and thus the total strain of the multilayer is not strongly affected. As a result, the stress in the TGO is not significantly affected by the bond coat CTE.

In addition to imparting good oxidation resistance, the bond coat must be compatible with the superalloy. As such, a bond coat with a higher Co concentration would be expected to be less susceptible to interdiffusion. Previous work on a Co-based superalloy substrate coated with a γ-β CoNiCrAlY by plasma spray revealed no significant change in microstructure and composition profiles after cyclic oxidation at 1100 °C [35].

Additionally, the CTE mismatch between the superalloy and the bond coat can induce rumpling under certain conditions that can promote TBC spallation [36, 37]. Rumpling is observed less frequently in land based turbines due to lower operating temperatures and the less frequent thermal cycling, nevertheless, NiCoCrAlY bond coats are susceptible to rumpling [38]. Thus, matching the CTE of the bond coat to the superalloy may favorably improve cyclic life. However, because rumpling is a complex process which depends on the materials properties of all of the components of the TBC, the effect of superalloy CTE on rumpling is not considered here [37].

5.3. Delamination of TBCs

Thermal expansion mismatch strains also develop in the multilayer TBC systems due to the low CTE of the TBC and the TGO. TBC systems may fail by a number of different mechanisms depending on the TBC composition, morphology, and experimental conditions [16, 39]. The multilayer used in the subsequent calculations is modeled after an APS-TBC used to protect the turbine blades in industrial turbines, where the thickness of the bond coat is on the order of 100 µm and failure typically occurs in the TBC directly above the TGO/TBC interface [15, 16].[3]

[3]The ERR is actually highest at the bond coat/TGO interface, but, because of the roughness of the bond coat, cracks do not typically grow to lengths that produce spallation.

The thermo-mechanical model was used to calculate G for propagation of an edge crack for a series of TBC systems and temperature excursions. The properties of the TBC system, consisting of a superalloy substrate, bond coat, TGO, and TBC, are listed in Table 3. Unless otherwise specified, the TBC thickness is fixed at 300 µm, typical of air plasma sprayed TBCs, and the TGO thickness is set to be 3 µm α-Al_2O_3.

The ERR for TBC delamination from the five Co-based alloys and one Ni-based alloy investigated was calculated as a function of dwell temperature, Figure 6(a). G increases monotonically with temperature for all of the alloys, as the thermal strain is proportional to $\Delta\alpha\Delta T$, which increases with exposure temperature. An inflection point is present in the G curve that corresponds to the γ'-solvus of the superalloy. To further compare the superalloys, G was calculated for TBCs cooled from 1100 to 25 °C as a function of mean CTE, with the mean CTE values of the six superalloys of interest labeled in Figure 6(b).

The thickness of the TBC will also affect the driving force for cracking. In Figure 7 the energy release rate is plotted as a function of TBC thickness for TBC systems cooled from 1100 °C. G increases nearly linearly with increasing TBC thickness. The linear increase in G with H_{TBC} is expected as the strain energy in the TBC is proportional to $(\Delta\alpha\Delta T)^2 E_{TBC} H_{TBC}$, where $\Delta\alpha$ is the CTE mismatch between the coating and the substrate and ΔT is the difference between the exposure temperature and the temperature at which delamination occurs.

The effect of CTE on TBC delamination calculated above is in agreement with the experimental results of Helminiak et al. [40], who investigated the thermal cycling lifetime of TBCs on superalloys with varying CTE and found that lifetime decreased with increasing superalloy CTE. The same investigators also found that increasing the TBC thickness on a given alloy also decreased lifetime, in agreement with the magnitude of G increasing with H_{TBC}, Figure 7.

The dependence of superalloy thermal expansion on TBC durability described above will also apply to the driving force for the delamination of EB-PVD TBCs. However, the properties of the bond coat, particularly the propensity for rumpling and the bond coat/TGO interfacial toughness, strongly affect durability of EB-PVD TBCs [41], and the influence of superalloy thermal expansion on the behavior of the bond coat would need to be considered

in such an analysis.

6. Implications for Co-based superalloy design

The thermal expansion data and thermo-mechanical calculations previously described give insight into the influence that alloy composition can have on the durability of coatings. When the oxidized superalloy is considered, the ERR for TGO delamination is approximately 1.5-2 × larger for the high CTE alloys; the Ternary, 2Ta, 6Ti and CoNi-A alloys exhibit higher ERRs compared to the low CTE alloys, René N5 and CoNi-E, if it is assumed that protective alumina forms following limited transient CoO oxidation. The oxidation resistance of the Ternary alloy has been found to be insufficient due to rapid CoO formation [4]. However, additions of Al and Ni in the CoNi-E alloy limit the amount of transient oxidation while also decreasing the CTE as shown in Figure 3. Cr additions are also known to improve oxidation resistance, but Cr markedly increased the CTE of the CoNi-A alloy and decreases the γ'-solvus [6]. Thus, to optimize durability under the thermal cycling conditions relevant to operation, alloy composition must be tailored to promote alumina formation and adherence, while minimizing CTE.

The mean CTE strongly depends on the volume fraction of γ'. The addition of γ'-forming elements, notably Ti, Ni, and Al, increases the volume fraction of the $L1_2$ phase and raises the γ'-solvus temperature, Figure 8. Overall, the mean CTE at 1000°C decreases with increasing γ'-solvus. However, the 6Ti and CoNi-E alloys stand out from this overall trend: the 6Ti alloy exhibits an anomalously high mean CTE, and the CoNi-E alloy exhibits an anomalously low mean CTE. This is likely due to the higher and lower melting temperatures (Table 2) of the 6Ti and CoNi-E alloys, respectively.

As with Ni-based alloys, bond coatings will likely be applied $L1_2$-containing Co-based alloys in many applications. Here we have shown that the CTE of the bond coat did not strongly affect the driving force for TGO delamination so that other factors, including interdiffusion with the superalloy and TGO adherence can be considered as design parameters for the optimal bond coat. The durability of these TBC systems is typically limited by TBC spallation that results from crack propagation in the TBC. As was shown in Figure 6, the driving force for delamination increases with superalloy mean CTE and thus developing

superalloys with high a volume fraction of γ' and a high γ'-solvus is expected to minimize the CTE mismatch with the TGO and the TBC, which drives cracking.

7. Conclusions

1. The mean CTEs of γ'-containing Co-based superalloys, the Ternary, 2Ta, 6Ti, and CoNi-A alloys, are higher than the Ni-based alloy René N5. One Co-based alloy, CoNi-E, possesses CTE similar that of René N5.
2. Generally, the mean CTE of both Ni- and Co-based γ-γ' superalloys decreases with increasing γ'-solvus temperature.
3. The energy release rate for TGO and TBC delamination is proportional to both coating thickness and to $((\alpha_{coating} - \alpha_{alloy})\Delta T)^2$, which is the mean CTE mismatch between the superalloy substrate and either the TGO and/or the TBC.
4. For intrinsic oxidation of the superalloy substrate, the driving force for cracking at the superalloy/TGO interface is about 1.5-2$\times$ greater for the high CTE alloys (the Ternary, 2Ta, 6Ti, and CoNi-A alloys) compared to René N5 and CoNi-E at $T = 1100\,^{\circ}\mathrm{C}$.
5. The effect of bond coat CTE on G for TGO delamination is much smaller than variations in superalloy CTE.
6. The driving force for delamination of the TBC is higher for the Ternary, 2Ta, 6Ti, and CoNi-A alloys compared to René N5 and CoNi-E.
7. Increasing the TBC thickness monotonically increases the driving force for delamination.
8. The driving force for delamination of the TBC increases proportionally with TBC thickness.

Acknowledgements: TMP and MST gratefully acknowledge the support of the National Science Foundation under NSF DMREF Grant DMR 1534264 and MRB and RWJ gratefully acknowledge the support of the National Science Foundation under Grant DMR 1105672.

References

[1] R. Reed, The Superalloys, Cambridge ed., Cambridge, 2006.

[2] J. Sato, T. Omori, K. Oikawa, I. Ohnuma, Cobalt-Base High-Temperature Alloys, Science 90 (2006).

[3] A. Suzuki, T. M. Pollock, High-temperature strength and deformation of γ/γ two-phase CoAlW-base alloys, Acta Mater 56 (2008) 1288–1297.

[4] T. Pollock, J. Dibbern, M. Tsunekane, J. Zhu, A. Suzuki, New Co-based γ-γ high-temperature alloys, JOM 62 (2010) 58–63.

[5] K. Tanaka, M. Ooshima, N. Tsuno, A. Sato, H. Inui, Creep deformation of single crystals of new CoAlW-based alloys with fcc/L12 two-phase microstructures, Philos Mag 92 (2012) 4011–4027.

[6] M. S. Titus, A. Suzuki, T. M. Pollock, High Temperature Creep of New L1 2 -containing Cobalt-base Superalloys, in: Superalloys 2012, 2012, pp. 823–832.

[7] M. S. Titus, A. Suzuki, T. M. Pollock, Creep and directional coarsening in single crystals of new γ-γ' cobalt-base alloys, Scr Mater 66 (2012) 574–577.

[8] F. Xue, H. Zhou, X. Chen, Q. Shi, H. Chang, M. Wang, X. Ding, Q. Feng, Creep behavior of a novel Co-Al-W-base single crystal alloy containing Ta and Ti at 982 C, MATEC Web of Conferences 14 (2014) 15002.

[9] A. Suzuki, H. Inui, T. M. Pollock, L12-strengthened cobalt-base superalloys, Ann Rev Mater Res (2015).

[10] M. Tsunekane, A. Suzuki, T. M. Pollock, Single-crystal solidification of new CoAlW-base alloys, Intermetallics 19 (2011) 636–643.

[11] N. Birks, G. H. Meier, F. S. Pettit, Introduction to the high temperature oxidation of metals, Cambridge University Press, 2006.

[12] G. H. Meier, F. S. Pettit, High-temperature corrosion of alumina-forming coatings for superalloys, Surf Coat Tech 39 (1989) 1–17.

[13] E. P. Busso, H. E. Evans, Z. Q. Qian, M. P. Taylor, Effects of breakaway oxidation on local stresses in thermal barrier coatings, Acta Mater 58 (2010) 1242–1251.

[14] A. Feuerstein, J. Knapp, T. Taylor, A. Ashary, A. Bolcavage, N. Hitchman, Technical and economical aspects of current thermal barrier coating systems for gas turbine engines by thermal spray and EBPVD: a review, J Thermal Spray Tech 17 (2008) 199–213.

[15] J. Toscano, R. Vaßen, A. Gil, M. Subanovic, D. Naumenko, L. Singheiser, W. J. Quadakkers, Parameters affecting tgo growth and adherence on MCrAlY-bond coats for TBC's, Surf CoatTech 201 (2006) 3906–3910.

[16] N. M. Yanar, M. A. Helminiak, G. H. Meier, F. S. Pettit, Comparison of the failures during cyclic oxidation of yttria-stabilized (7 to 8 weight percent) zirconia thermal barrier coatings fabricated via electron beam physical vapor deposition and air plasma spray, Metall Mater Trans A 42 (2011) 905–921.

[17] J. Zhu, M. S. Titus, T. M. Pollock, Experimental Investigation and Thermodynamic Modeling of the Co-Rich Region in the Co-Al-Ni-W Quaternary System, Journal of Phase Equilibria and Diffusion (2014).

[18] R. F. Speyer, Thermal analysis of materials, CRC Press, 1993.

[19] M. S. Titus, High temperature deformation mechanisms of $L1_2$-containing Co-based superalloys, Ph.D. thesis, University of California, Santa Barbara, 2015.

[20] C. Walter, B. Hallstedt, N. Warnken, Simulation of the solidification of CMSX-4, Mater Sci Eng: A 397 (2005) 385–390.

[21] M. Ooshima, K. Tanaka, N. L. Okamoto, K. Kishida, H. Inui, Effects of quaternary alloying elements on the γ solvus temperature of CoAlW based alloys with fcc/L12 two-phase microstructures, J Alloy Compd 508 (2010) 71–78.

[22] Y. S. Touloukian, R. K. Kirby, R. E. Taylor, P. D. Desai, Thermophysical Properties of Matter-the TPRC Data Series. Volume 12. Thermal Expansion Metallic Elements and Alloys, Technical Report, DTIC Document, 1975.

[23] J. W. Hutchinson, Z. Suo, Mixed mode cracking in layered materials, Adv appl mech 29 (1992) 191.

[24] R. W. Jackson, M. R. Begley, Critical cooling rates to avoid transient-driven cracking in thermal barrier coating (TBC) systems, Inter J Solids Structures 51 (2014) 1364–1374.

[25] A. G. Evans, D. R. Clarke, C. G. Levi, The influence of oxides on the performance of advanced gas turbines, J Euro Ceram Soc 28 (2008) 1405–1419.

[26] P. Hou, Segregation phenomena at thermally grown Al_2O_3/alloy interfaces, Annu. Rev. Mater. Res. 38 (2008) 275–298.

[27] Z. Suo, J. W. Hutchinson, Interface crack between two elastic layers, Inter J Fracture 43 (1990) 1–18.

[28] L. Klein, A. Bauer, S. Neumeier, M. Göken, S. Virtanen, High temperature oxidation of γ/γ-strengthened Co-base superalloys, Corros Sci 53 (2011) 2027–2034.

[29] G. R. Wallwork, A. Z. Hed, Mapping of the oxidation products in the ternary Co-Cr-Al system, Oxid Met 3 (1971) 213–227.

[30] C. S. Giggins, F. S. Pettit, Oxidation of Ni-Cr-Al alloys between 1000° and 1200°C, J Electrochemical Soc 118 (1971) 1782–1790.

[31] B. A. Pint, The role of chemical composition on the oxidation performance of aluminide coatings, Surf Coat Tech 188 (2004) 71–78.

[32] R. W. Jackson, D. M. Lipkin, T. M. Pollock, The oxidation and rumpling behavior of overlay B2 bond coats containing Pt, Pd, Cr and Hf, Surf Coat Tech 221 (2013) 13–21.

[33] T. A. Taylor, P. N. Walsh, Thermal expansion of MCrAlY alloys, Surf Coat Tech 177 (2004) 24–31.

[34] J. A. Haynes, B. A. Pint, W. D. Porter, I. G. Wright, Comparison of thermal expansion and oxidation behavior of various high-temperature coating materials and superalloys, Mater High Temp 21 (2004) 87–94.

[35] N. Vermaak, A. Mottura, T. Pollock, Cyclic oxidation of high temperature coatings on new γ-strengthened cobalt-based alloys, Corros Sci 75 (2013) 300–308.

[36] A. G. Evans, D. R. Mumm, J. W. Hutchinson, G. H. Meier, F. S. Pettit, Mechanisms controlling the durability of thermal barrier coatings, Prog Mater Sci 46 (2001) 505–553.

[37] D. S. Balint, J. W. Hutchinson, Undulation instability of a compressed elastic film on a nonlinear creeping substrate, Acta Mater 51 (2003) 3965–3983.

[38] C. Mercer, K. Kawagishi, T. Tomimatsu, D. Hovis, T. M. Pollock, A comparative investigation of oxide formation on EQ (equilibrium) and NiCoCrAlY bond coats under stepped thermal cycling, Surf Coat Tech 205 (2011) 3066–3072.

[39] C. G. Levi, J. W. Hutchinson, M.-H. Vidal-Sétif, C. A. Johnson, Environmental degradation of thermal-barrier coatings by molten deposits, MRS bulletin 37 (2012) 932–941.

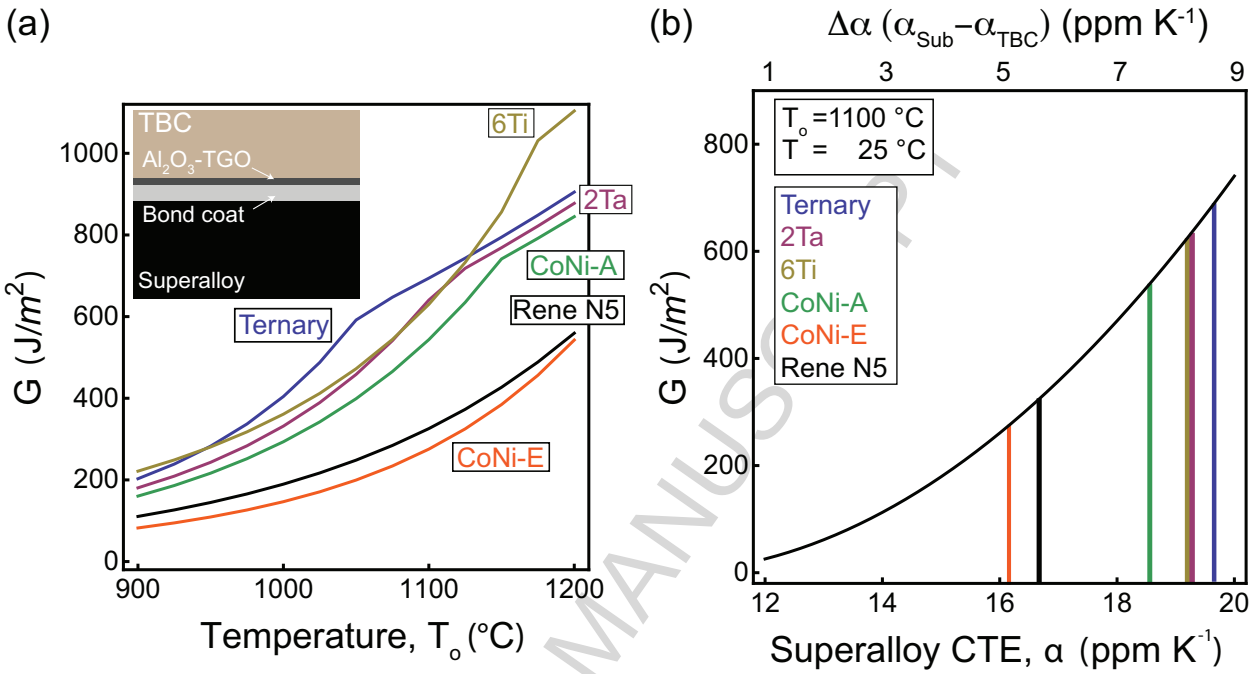

Figure 6: (a) The energy release rate, G, for cracking at the TGO/TBC interface for 300 µm thick TBCs cooled to T =25 °C, as a function of initial temperature, T_o, for a series of superalloy substrates. (b) The energy release rate, G, for cracking at the TGO/TBC interface for 300 µm thick TBCs following cooling from T_o=1100°C to T =25 °C as a function of substrate CTE. The mean CTE at 1100°C of the six superalloys considered in this investigation are overlaid.

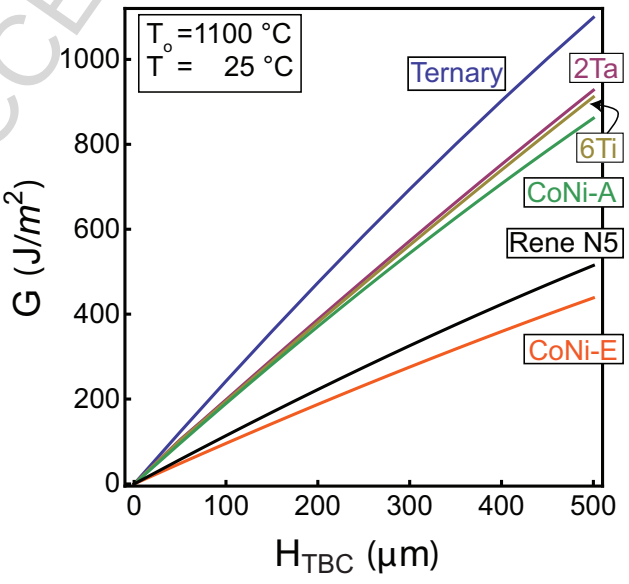

Figure 7: The energy release rate, G, for cracking at the TGO/TBC following cooling from T_o =1100 °C to T =25 °C as a function of TBC thickness, H_{TBC} on Ternary, 2Ta, 6T, CoNi-A, CoNi-E, and René-N5 substrates, each coated with 100 µm CoNiCrAlY bond coat that grown a 3 µm Al_2O_3 scale.

8. Tables

Table 1: Composition of the alloys investigated (at.%) along with a bond coat composition used in the mechanical analysis.

Alloy	Co	Ni	Al	W	Ta	Ti	Cr
Ternary	79.9	-	9.4	10.7	-	-	
2Ta	79.4	-	8.8	9.8	2.0	-	-
6Ti	79.0	-	6.7	8.1	-	6.2	-
CoNi-A	45.9	29.2	9.8	6.3	2.4	-	6.4
CoNi-E	49.9	29.6	11.2	6.5	2.8	-	-
René N5	7.6	65	13.7	1.6	2.2	-	8
NiCoCrAlY	23.7	35.7	14.4	25.9	-	-	14.4

Table 2: Polynomial fit of CTE data. † from Ref. [19] and ‡ from Ref. [20].

	$\alpha(T) = A + BT + CT^2 + DT^3 + ET^4$					T_{solvus}	T_m
Alloy	A	10^{-3} BT	10^{-5} CT^2	10^{-8} DT^3	10^{-11} ET^4	(°C)	(°C)
Ternary	12.93	-5.31	3.72	−5.80	3.14	1039	1447†
2Ta	9.422	13.6	-0.736	-0.87	1.05	1103	1407†
6Ti	13.84	-6.58	3.63	-4.82	2.25	1163	1231†
CoNi-A	14.18	-4.32	1.03	-0.936	0.625	1147	1380†
CoNi-E	9.84	-6.84	0.25	-1.36	0.951	1182†	1396†
René N5	13.46	-2.01	0.491	-0.318	0.261	1305‡	1326‡
NiCoCrAlY	12.09	2.35	0.512	-0.48	0.121	-	-

Table 3: Properties of TBC system constituents

Layer	Thickness (µm)	E (GPa)	ν	α ($10^{-6}\,K^{-1}$)
Superalloy	3000	150 − 250	0.3	15-20
Bond coat	100	180	0.3	18
Al_2O_3	3	400	0.25	8
CoO	10	200	0.25	15
TBC	300	40	0.2	11

9. Figures

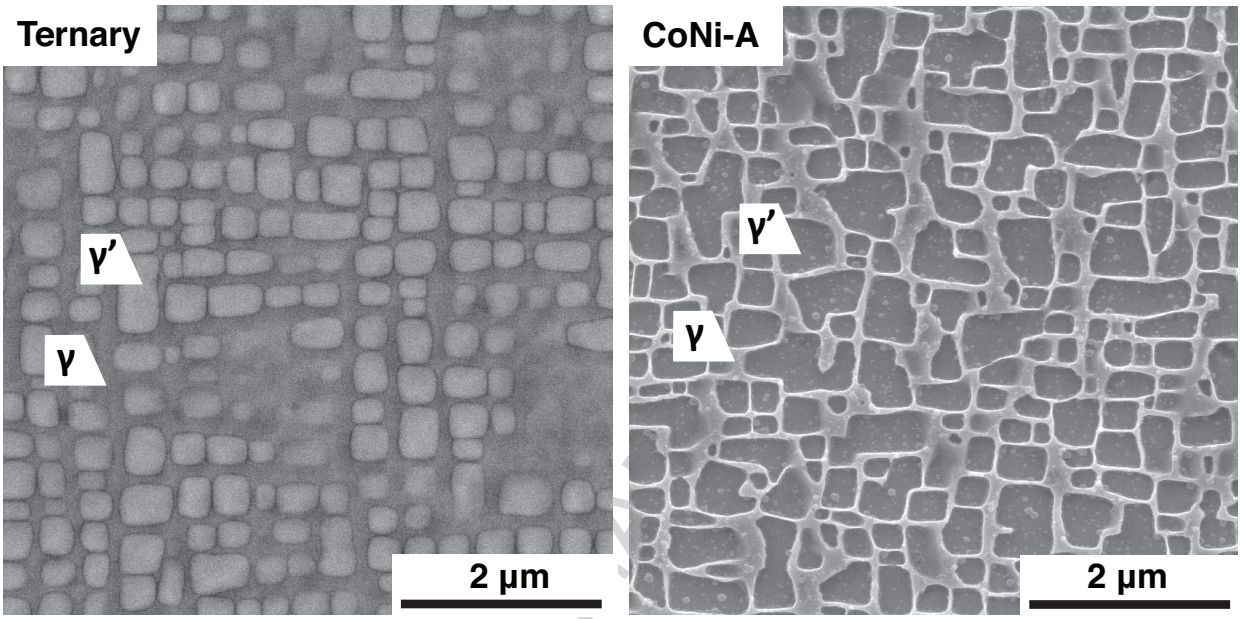

Figure 1: Backscatter scanning electron microscopy images of the aged Ternary and CoNi-A alloys in the etched condition. In order to grow and coarsen the γ' precipitates, aging heat treatments were conducted at 950°C/12 h and 950°C/100 h for the Ternary and CoNi-A alloys, respectively.

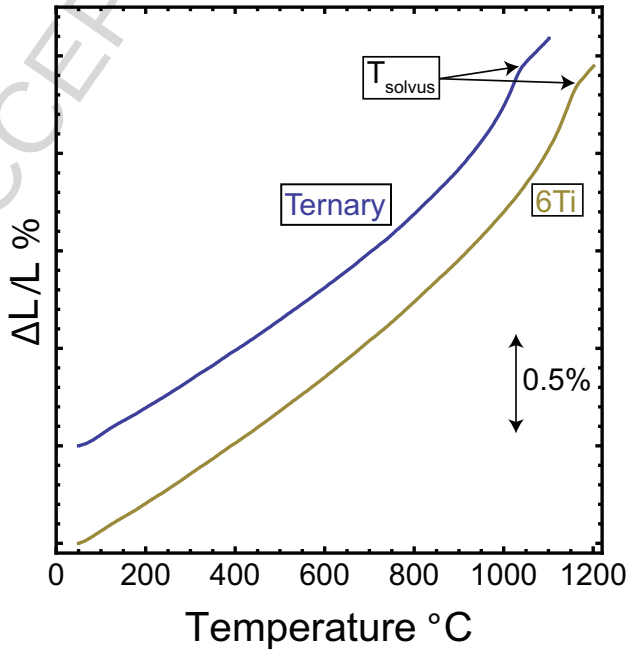

Figure 2: Measured thermal strain for the Ternary and 6Ti alloys. The 6Ti is offset 0.5%. A scale bar marking 0.5% strain is present.

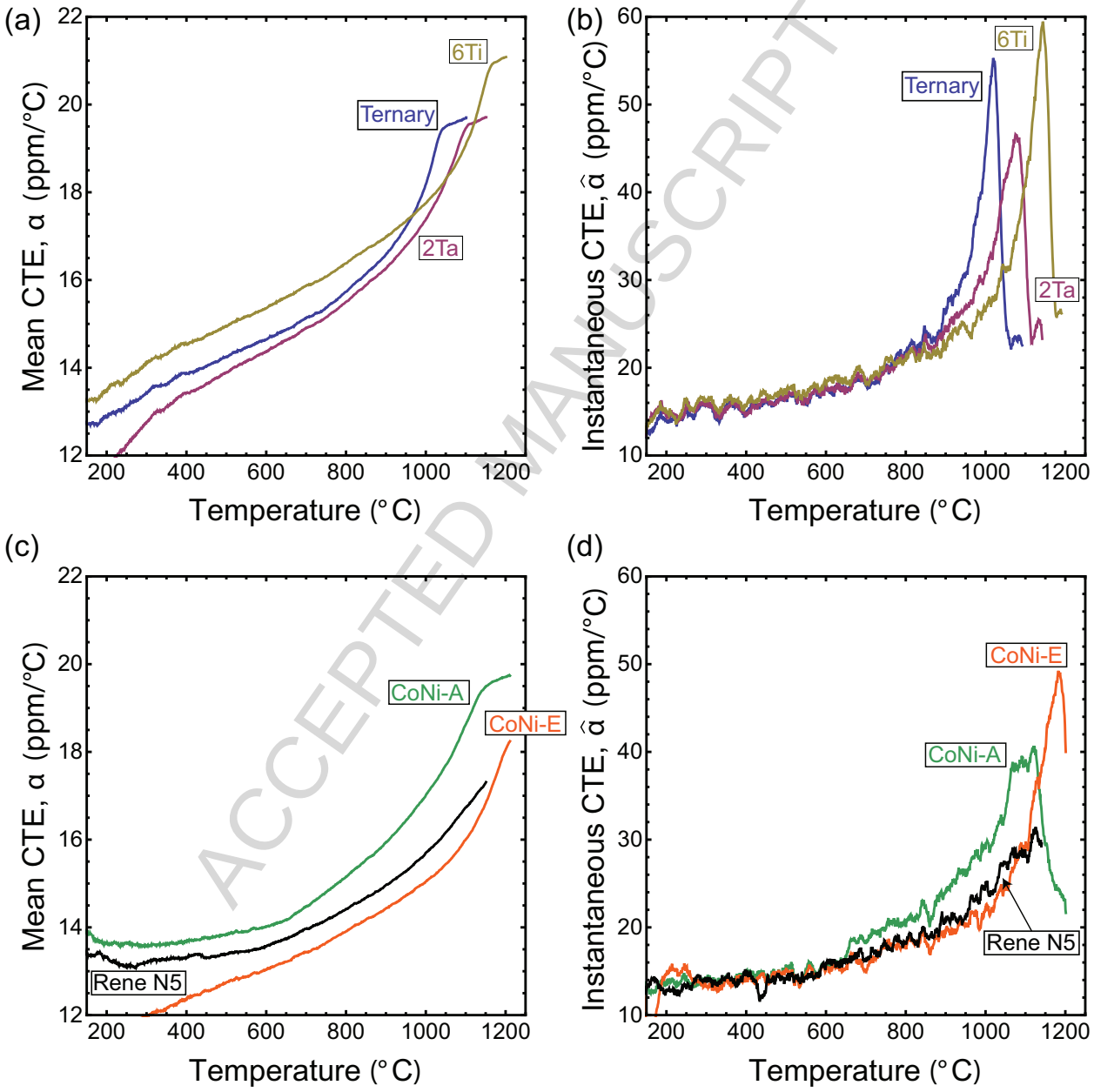

Figure 3: Thermal displacements measured in dilatometer were used to calculate the mean CTE, α, (a) and (c) and the expansivity $\hat{\alpha}$ of the Ternary, 2Ta, 6Ti, CoNi-A, CoNi-E, and René N5 alloys (b) and (d). α_{2Ta} in the region of the γ'-solvus is inlaid in (a) where the gray dashed lines given by the linear fit of the curve above and below the solvus are used to determine the solvus temperature.

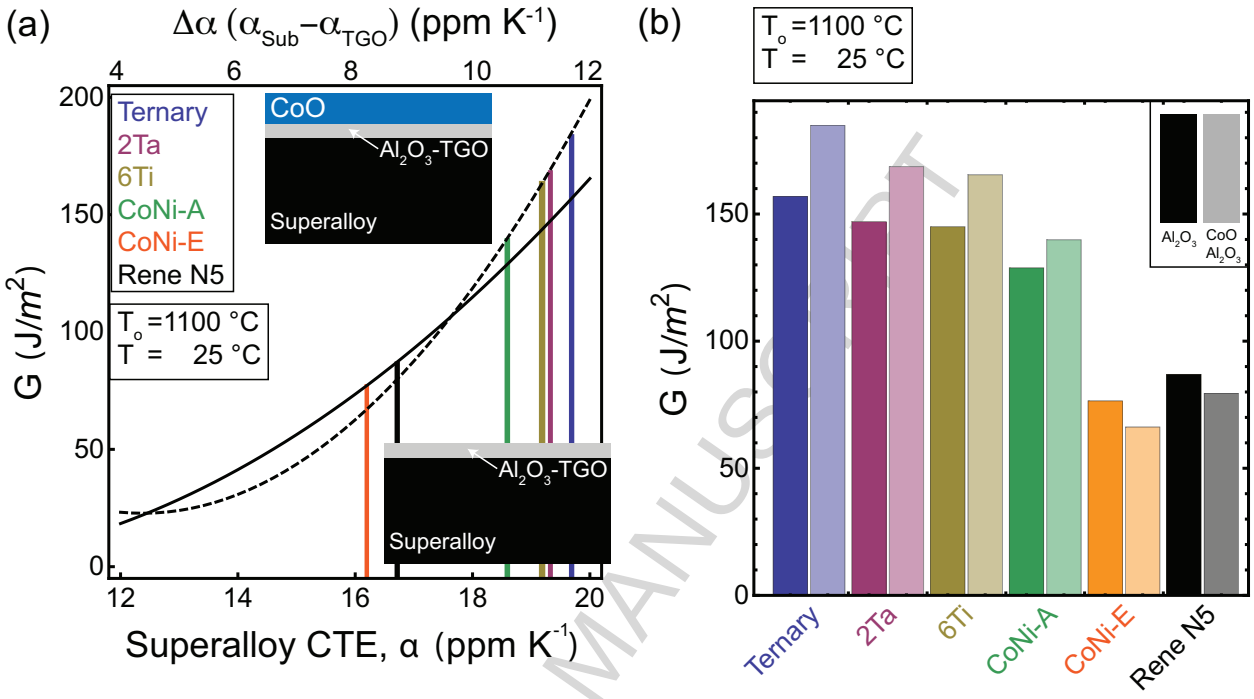

Figure 4: The energy release rate, G, for cracking at the superalloy/TGO interface for a 3 µm thick Al_2O_3 TGO (solid line) and for a bilayer Al_2O_3-CoO TGO (dashed line), where the $H_{Al_2O_3}$=3 µm and H_{CoO}=10 µm cooled from T_o=1100°C to T =25 °C, as a function of superalloy mean CTE. The value of the mean CTE at 1100 °C of the six superalloys considered in this investigation are overlaid in (a) and presented in the bar chart in (b).

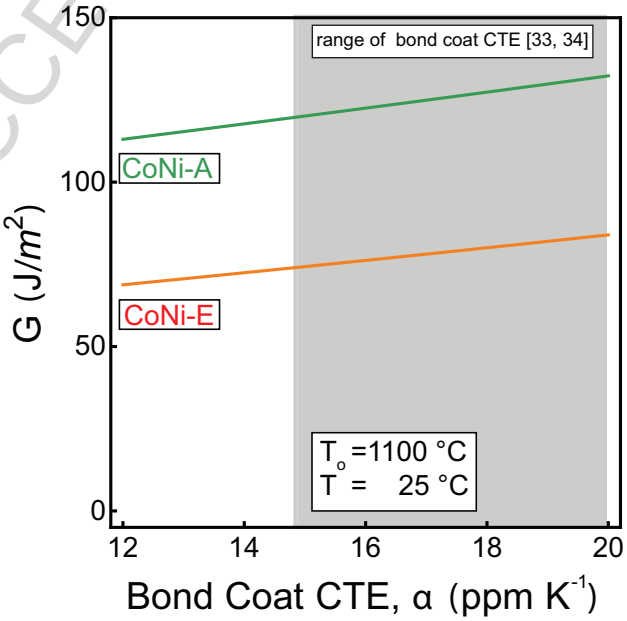

Figure 5: The energy release rate, G, for cracking at the bond coat/TGO interface for 3 µm thick TGO cooled T_o=1100°C to T =25 °C, as a function of bond coat CTE. G is presented for bond coats on CoNi-A and CoNi-E alloys.

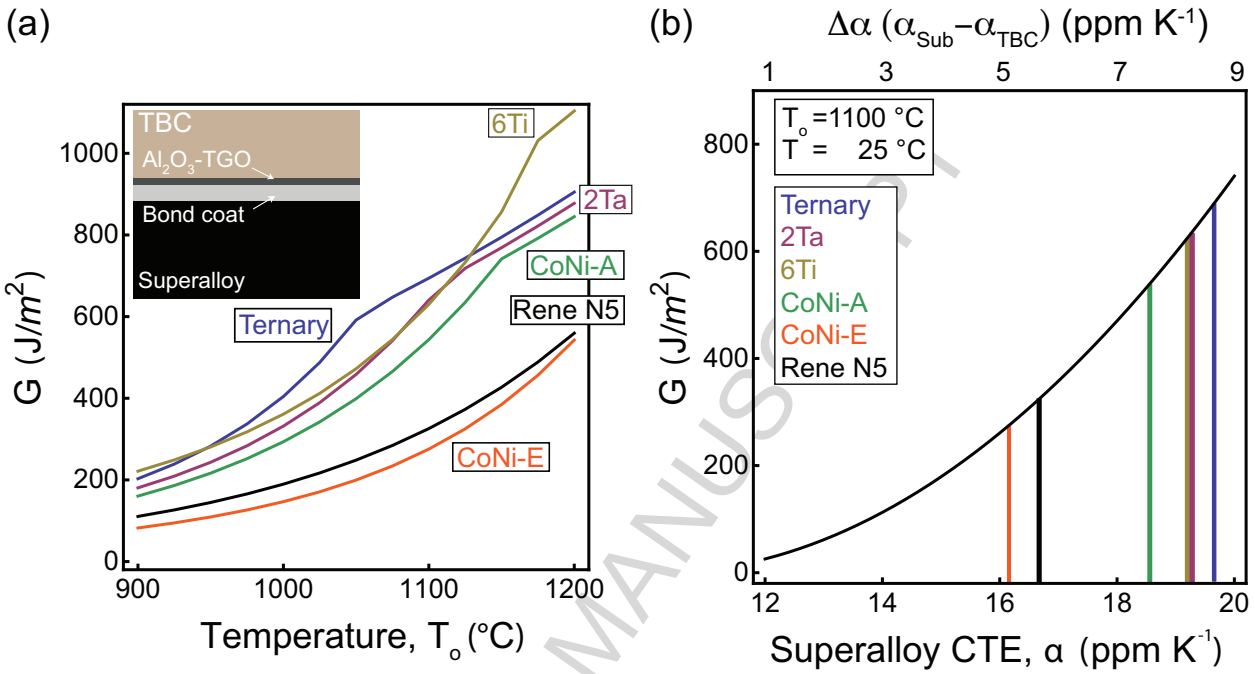

Figure 6: (a) The energy release rate, G, for cracking at the TGO/TBC interface for 300 µm thick TBCs cooled to T =25 °C, as a function of initial temperature, T_o, for a series of superalloy substrates. (b) The energy release rate, G, for cracking at the TGO/TBC interface for 300 µm thick TBCs following cooling from T_o=1100°C to T =25 °C as a function of substrate CTE. The mean CTE at 1100°C of the six superalloys considered in this investigation are overlaid.

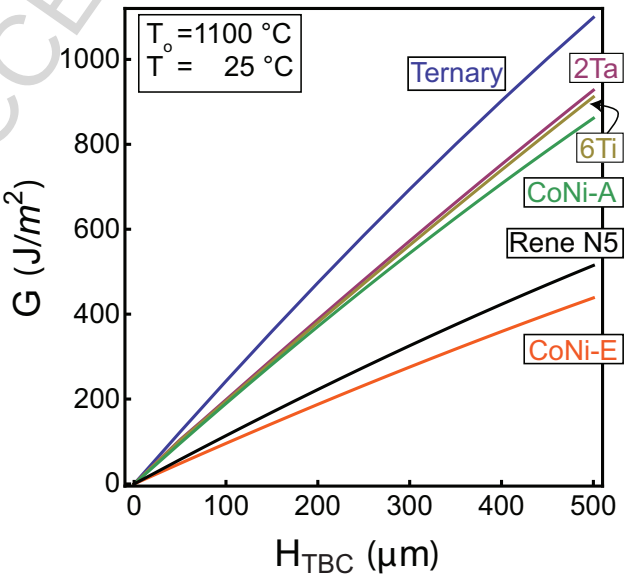

Figure 7: The energy release rate, G, for cracking at the TGO/TBC following cooling from T_o =1100 °C to T =25 °C as a function of TBC thickness, H_{TBC} on Ternary, 2Ta, 6T, CoNi-A, CoNi-E, and René-N5 substrates, each coated with 100 µm CoNiCrAlY bond coat that grown a 3 µm Al_2O_3 scale.

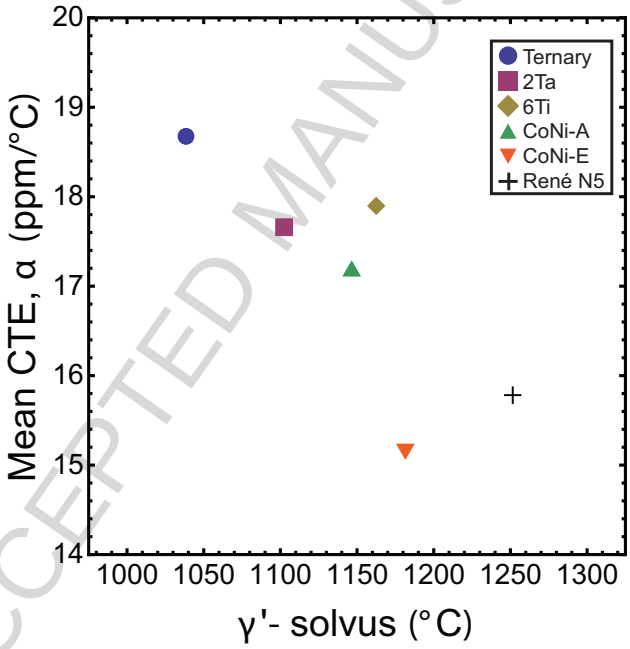

Figure 8: Mean CTE, α, at 1000°C plotted vs. the γ'-solvus of the alloys investigated here. The mean CTE generally decreases with increasing γ'-solvus. Exceptions are found when the melting temperature for the alloy is significantly lower or higher, as in the case for the 6Ti and CoNi-E alloys.

Highlights

- The thermal expansion behavior and the γ' solvus was determined for a series of precipitation strengthen Co-based γ/γ' alloys.
- The driving force for the delamination of oxide scales that could grow on the alloys was calculated.
- The driving force for the delamination of thermal barrier coatings from these alloys was calculated.
- The implications of alloy composition on thermal expansion and the effect of thermal expansion on the durability of coatings is discussed.